The efficacy of the quercetin analogue LY294002 in immortalized cancer cell lines is related to the oxygenic and metabolic status of cells

Xinyue Huang[1], Michelle Potter[2], Ben Pilgrim[3], Ruchuta Ardkhean[4], Mikail Kabeshov[3], Timothy Claridge[3], Matthew Wiseman[5], Karl Jonathan Morten[2], Timothy Donohoe[3], Helen Elizabeth Townley[2]

[1]Engineering Science, Oxford University, Oxford, United Kingdom
[2]Obstetrics and Gynecology, Oxford University, Oxford, United Kingdom
[3]Chemistry, Oxford University, Oxford, United Kingdom
[4]Department of Radiation Oncology, Oxford University, Oxford, United Kingdom
[5]Department of Radiation Oncology, NIM Genetics, Madrid, Spain

Original Article

Abstract

Purpose: LY294002, a promising drug for chemotherapy, suppresses the activity of Phosphatidylinositol 3-Kinase (PI3K) which is pivotal to a number of processes such as proliferation, metabolism, and apoptosis. The compound has, however, been seen to have very variable efficacy *in vivo*. **Methods:** Proliferation and viability of two immortalized cells with divergent bioenergetic profiles was determined using crystal violet staining, and the 3-(4, 5-dimethylthiazol-2yl)-2, 5-diphenyl tetrazolium bromide (MTT) assay. Oxygen consumption rates were determined using MitoXpress-Xtra probes, and lactate generation was assessed with pH-Xtra probe and BM-lactate strips. Immunoblotting was performed with phospho-Akt-Ser 473 and Akt-pan primary antibodies. **Results:** U87 cells were shown to have a glycolytic metabolism, whereas RD cells exhibited a more aerobic metabolism. In both lines, hypoxia was shown to increase lactate production, and LY294002 reduced lactate production. The drug decreased cell proliferation and viability under all conditions, but the effect was greatest in U87 cells under normoxic conditions. **Conclusion:** Metabolic analysis showed a link between a glycolytic cell status and LY294002 induced cell death. However, in both cell lines the drug was also less effective under hypoxic conditions, as would be found in a tumour *in vivo*. Furthermore, in the presence of LY294002 the phosphorylation status of Akt, a target of PI3K, was found to be related to both the mechanism of cell respiration, and the oxygenic status of the cells.

Keywords: Apoptosis, Cancer, Hypoxia, Quercetin, Metabolism, PI3K

1. Introduction

LY294002, a quercetin analogue, is recognized as a potent anticancer drug.[1] In this study we investigate whether there is a link between the oxygenic and metabolic status of the cancer cell and the efficacy of LY294002. To maintain high proliferative levels cancer cells need to re-programme their energy metabolism to allow proliferation under reduced levels of oxygen and nutrients.[2] Maintaining growth under hypoxic conditions and evading apoptosis have been strongly linked to changes in metabolic behaviour.[3] Cancer cell metabolism is very adaptable; switching between glycolytic and oxidative phosphorylation depending upon oncogenic mutation status and the tumor microenvironment.[4]

LY294002 suppresses the activity of phosphatidylinositol 3-kinase (PI3K) *via* competitive inhibition of an adenosine triphosphate (ATP) binding site on the p85a subunit.[5] Akt is a well-characterized effector of PI3K, and is activated by both translocation to

the plasma membrane and phosphorylation at Thr 308 and Ser 473.[6,7] Thr 308 phosphorylation (by phosphoinositide-dependent kinase-1; PDK1) is necessary and sufficient for Akt activation but maximal activation requires additional phosphorylation at Ser 473.[8] The PI3K/Akt pathway exhibits control over proliferation, migration, metastasis, metabolism, apoptosis, and angiogenesis, and is therefore a target for anticancer agents.[1]

The metabolic profiles of cells are affected by the oxygen and glucose concentration of their environment, with cells on the periphery of tumors growing more quickly than those in the centre.[9,10] The Warburg model states that cancer cells use higher levels of glucose than normal cells, and show increased lactate generation. However, this may not be a universal truth for all cancers, and could have implications for therapeutics which target cancer cell metabolism.[11] Herein, we have therefore assessed the effect of LY294002 under normoxic and hypoxic conditions and in cell lines with different metabolic profiles.

2. Methods and Materials

2.1. Cell culture
Cells were plated at a density of 1×10^4 cells per well (96-well plate, Nunc) in 200 μL of growth medium (Dulbecco's Modified Eagle's Medium (DMEM)) including 25 mM glucose, 1 mM pyruvate [Sigma]), supplemented with 10% foetal bovine serum [Sigma], 2 mM L-Glutamine [Gibco], 100Ū/mL Penicillin and 0.1 mg/mL Streptomycin [Gibco]) in 96-well plates and incubated at 37 °C in 5% CO_2 atmosphere. Cells grown under hypoxic conditions were incubated in 1% O_2 and 5% CO_2.

Two cell lines, U87 (American Type Tissue Culture Collection (ATCC) number HTB14, glioblastoma astrocytoma) and RD (ATCC number CRL-7763, rhabdomyosarcoma), were selected on the basis of their very different metabolic phenotypes *in vitro* when cultured on different concentrations of glucose. The RD cell line shows a consistently high level of oxidative phosphorylation on both high (25 mM) and low glucose media (1 mM) while U87 shows a low level of oxidative phosphorylation on high glucose which can be significantly increased by growth on low glucose media.[9] Both cell lines show reduced media acidification/ lactate production on 1mM glucose.

2.2. Crystal violet assay
Cell number was assessed using crystal violet (CV) staining. CV is a triphenylmethane dye which intercalates with DNA in a similar manner to ethidium bromide but is less mutagenic and detectable in the visible range. CV staining therefore provides a simple method for obtaining quantitative data on the number of cells based on the absorbance of the dye by DNA in the

cells. Cells were rinsed with pre-warmed PBS and fixed with 1% glutaraldehyde solution for 30 min. Fixed cells were stained with crystal violet solution (1% crystal violet [Sigma] dissolved in a mixture of methanol: glacial acetic acid: H_2O, 5:1:4 v/v/v) for 1 hour at room temperature. After staining, the supernatant was removed and cells washed carefully three times with water. The plate was then drained and dried overnight. Before reading, 100 μL solubiliser (1% sodium dodecyl sulfate in 10% glacial acetic acid) was added to each well and resuspended vigorously. The absorbance was read at 540 nm.

2.3. MTT assay
MTT is a colorimetric assay based on the capacity of the cellular mitochondrial dehydrogenase in living cells to reduce the yellow water-soluble substrate 3-(4, 5-dimethylthiazol-2yl)-2, 5-diphenyl tetrazolium bromide (MTT) into a dark blue/purple formazan product which is insoluble in water. Cells were washed twice with pre-warmed PBS and 100 μL 0.5 mg/mL MTT solution (0.5 mg/mL dissolved in a mixture of phosphate buffered saline (PBS): growth medium, 1:9 v/v) was added to each well and incubated at 37 ºC, in darkness. After 4 hours incubation the supernatant was removed and the MTT solubilized with 100 μL dimethyl sulfoxide per well. The absorbance was read at 570 nm.

2.4. Extracellular pH assay
The phosphorescence of pH-Xtra probe [Luxcel Biosciences] increases as lactic acid is produced and the media pH decreases. The pH–Xtra probe provides data on the rate at which pyruvate is converted to lactic acid with changes in fluorescence linked to the glycolytic activity of cells. The assay was carried out on cells incubated in clear bottom black tissue culture plates (BD falcon) and carried out according to manufacturers' instructions. The buffer solution was modified from the standard method to remove the potassium phosphate (20 mM glucose, 70 mM NaCl, 50 mM KCl, 0.8 mM $MgSO_4$, and 2.4 mM $CaCl_2$; pH7.4). Changes in time resolved fluorescence are monitored in a BMG Omega plate reader, using filters TR-exl (excitation) and 615 nm (emission). The lifetime is measured using dual delay time resolved measurements. The delay times for pH-Xtra are 100 and 300 μsec. The raw data produced is a graph of time (x-axis) versus TR-F intensity (y-axis). These measured TR-F intensity signals need to be converted into phosphorescence lifetime values. This is performed using the following equation:

$$\text{Lifetime } \tau \text{ (μs)} = \frac{t2 - t1}{L \left(\frac{D2}{D1} \right)}$$

Here t2 – t1 is delay time which is set to 200 μs, D1 and D2 are measured intensity value at time point t1 and t2. Once the lifetime curves have been calculated it is possible to determine the extracellular acidification rate

of the samples by looking at the difference in the lifetime values (rate of change) between two set time points.

Extracellular acidification rates (ECAR) are calculated from the linear part of the assay before a plateau is reached.

2.5. Lactate assay
Lactate generation was evaluated with BM-lactate strips [Roche]. For each sample, 25 μL media was added on to the reactive pad of a new lactate strip. The result was read by an Accutrend Lactate Meter [Roche] after incubation for 1 min.

2.6. Immunoblotting
Treated cells were lysed with tissue extraction buffer (50 mM Tris-HCl (pH 7.4), 150 mM NaCl, 1 mM ethylenediaminetetraacetic acid (EDTA), 1% Triton X-100, 0.1% sodium dodecyl sulfate (SDS), add 1 tablet of protease inhibitor in every 10 mL buffer before use). The lysates were quantified with the Pierce BCA protein assay kit (Thermo Scientific), mixed with loading buffer (Invitrogen) and reduced buffer (Invitrogen), and heated to 95 ℃ for 5 min before being analyzed by sodium dodecyl sulfate polyacrylamide gel electrophoresis (SDS-PAGE; 8-16% Precise Protein Gel; Thermo Scientific). Gels were transferred to nitrocellulose paper (Amersham) in transfer buffer (200 mM Glycine, 25 mM Tris, 20% Methanol) at 100 V for 1 hour. Membranes were blocked in Tris-buffered saline with 0.1% Tween 20 (TBST) containing 5% powdered milk at 4 ℃ overnight.

After washing with TBST buffer, membranes were incubated for 1 hour at 4 ℃ with primary antibodies; Phospho-Akt-Ser473 (pAkt-ser473, Cell Signaling), and Akt (pan) (Cell Signaling). The appropriate HRP-conjugated secondary antibody (Invitrogen) was used and the proteins on membranes were detected using the ECL Western Blotting Analysis System (Amersham) and autoradiography film (Hyperfilm ECL from Amersham Biosciences).

The band intensity on immunoblots was quantified using Image J software. On each blot, the density of both pAkt-ser473 and Akt (pan) were divided by the density of the house-keeping protein β-actin. Samples were then normalized against β-actin. Values are expressed as % of the zero drug control.

2.7. Statistical analysis
Where data is presented as an average value, error bars are shown as standard deviation of the mean. Data was analysed by the one–tailed student t-test: one star (*) for p values ≤ 0.05, two stars (**) for p values ≤ 0.01, and three stars (***) for p values ≤ 0.001.

3. Results

3.1. Immortalized cancer cell lines have different bioenergetics profiles
Immortalized cancer cell lines vary greatly in their bioenergetics profiles. We have previously measured the oxygen consumption rate (OCR) and extracellular acidification rate (ECAR) for a number of cell lines, in order to quantify mitochondrial respiration, and to give an indication of glycolysis.[9] For this study we therefore chose to look at the response of two bio energetically different cell lines at the extremes of our OCR v ECAR metabolic analysis; an aerobic line (RD) and a glycolytic line (U87).

The U87 and RD cell lines were subjected to Next Generation Sequence analysis of hotspot regions of 50 oncogenes and tumor suppressor genes (Supplementary Table 1). The metabolic status of the two chosen lines was further characterized by ^{13}C-NMR (Supplementary Figure 2).

3.2. The reduction in cell proliferation caused by LY294002 is much less marked under hypoxic conditions
Cells were incubated with LY294002 at micromolar concentrations up to 50 μM in RD and U87 cells. The efficacy of the LY294002 drug in reducing cell proliferation was assessed using the CV assay. RD cells incubated with LY294002 under normoxic conditions showed a decrease in cell number with increasing drug dose, and at the maximum dose of 50 μM the drug can be seen to reduce cell proliferation by approximately 27.0 % ± 3.2 (Figure 1a). U87 cells showed a more dramatic response to LY294002 under the same conditions, showing approximately 61.3% ± 1.3 decrease in cell proliferation at 50 μM drug (Figure 1b). Both reductions in cell number were shown to be statistically significant.

Under hypoxic (1% O$_2$) conditions and incubation with 50 μM LY294002 RD cells showed a reduction of only 13.4% ± 5.2 (Figure 1a), while under the same conditions U87 cells showed a reduction of 17.5% ± 12.5, although neither reduction was statistically significant (Figure 1b).

Therefore the two cell lines show both different sensitivity to the drug and altered sensitivity under reduced oxygen conditions. The fact that both cell lines were less susceptible to the drug under the hypoxic conditions underlines the importance of using test conditions that are as close as possible to the *in vivo* conditions.

In addition to determining proliferation, the viability of cells treated with LY294002 was assessed using the MTT assay. RD cells showed a reduction in metabolic

activity of 23.1% ± 4.3 under normoxic conditions, and an 11.1% ± 1.5 reduction in metabolism under hypoxic conditions, when incubated with 50 μM LY294002 (Figure 2a). U87 cells demonstrated a much more marked reduction in metabolism under normoxic conditions, with a reduction of 72.4 % ± 2.6 compared to control. Under hypoxic conditions, cells were much less affected with a reduction in metabolism of 30.9 % ± 4.0 (Figure 2b). Hence, the same trend is seen in terms of both proliferation and metabolism of cells.

3.3. Lactate production under both normoxic and hypoxic conditions, is decreased by LY294002
Levels of lactate, an established product of glycolysis, were determined in the culture media of RD and U87 cells under both normoxic and hypoxic conditions (Figure 3). Under both normoxic and hypoxic conditions

RD cells generated considerably less lactate than U87 cells. Under hypoxic conditions lactate levels increased in RD cells, but not U87 cells.

The addition of drug showed significant reductions in lactate generation for both cell lines under both normoxic and hypoxic conditions. Under normoxic conditions the drug reduced lactate in RD cells to undetectable levels, and U87 cells showed a 55.70 % ± 0.08 reductions compared to control levels (Figure 3). Under hypoxia, RD cells showed a 42.76 ± 0.04% reduction and U87 cells 66.00 ± 0.03% reduction in lactate concentration compared to normoxic levels (Figure 3). These results would be consistent with a slowing of glycolysis which would be expected if the PI3K pathway were inhibited by LY294002.
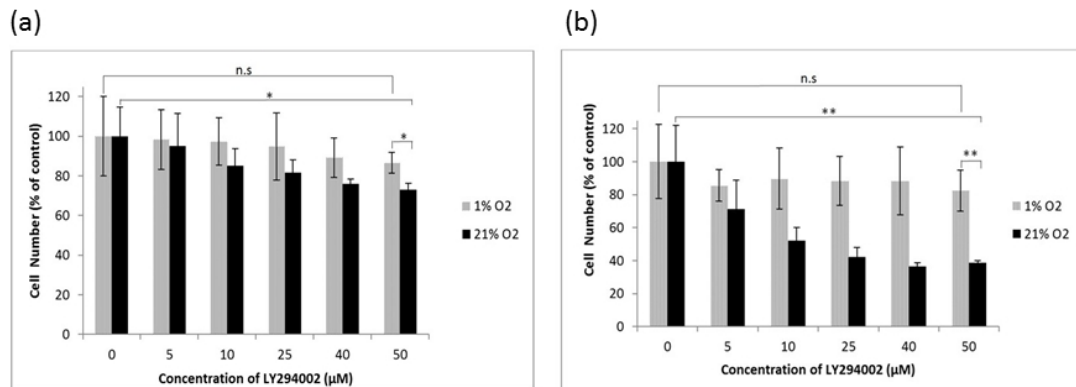

Figure 1: Cell number assessed using crystal violet staining, in the presence of increasing concentrations of LY294002, under either 1% or 21% oxygen, after incubation for 24 hours (a) RD cells (b) U87 cells. Figure shows a representative result of independent experiments, herein n=3, ± standard deviation (SD) mean. Significance was determined by the one-tailed student t-test.
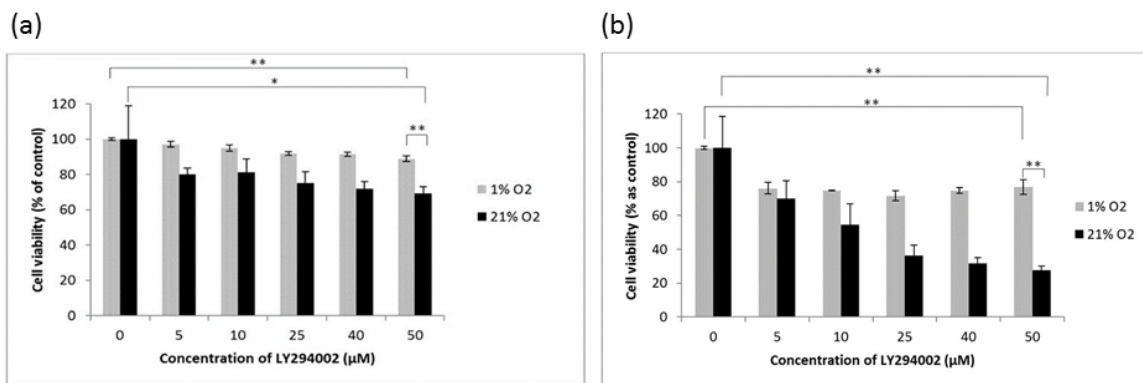

Figure 2: Cell metabolism assessed using MTT assay, in the presence of increasing concentrations of LY294002, either under 1% or 21% oxygen, after incubation for 24 hours (a) RD cells (b) U87 cells. Figure shows a representative result of independent experiments, herein n = 3 for each variable, ± SD mean. Significance was determined by the one-tailed student t-test.
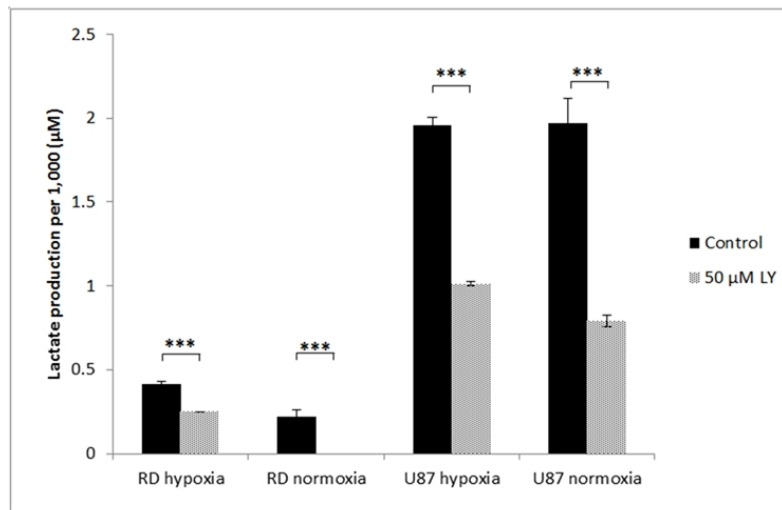
Figure 3: Lactate detected in the culture medium after 24 hours in the presence and absence of LY294002 for RD and U87 cells under 1% and 21% oxygen. The results were calibrated with relative cell number. (Using Student's t test, *** P < 0.001; the data are presented as the means ± standard deviation, n = 3)
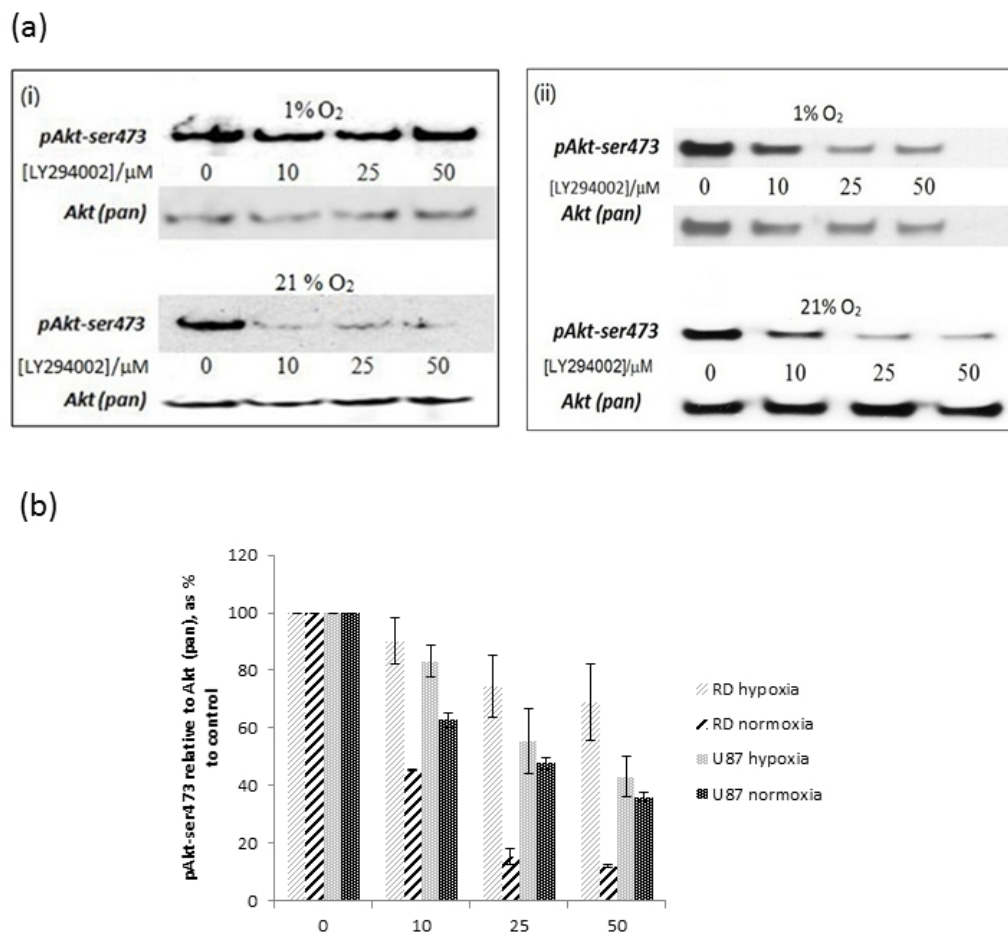

Figure 4: (a) Representative immunoblot of cell lysates from cells incubated with increasing amounts of LY294002 under either 1% O2 or 21% O2 (i) RD cells (ii) U87 cells. Blots were probed with anti-Akt (pan) or anti-pAkt-ser473 antibodies (b) Densitometry data taken from immunoblots shown in panel 'a'.

6   Huang *et al.*: Quercetin analogue LY294002 in immortalized cancer cell lines   *International Journal of Cancer Therapy and Oncology*

www.ijcto.org

3.4. Phosphorylation status of Akt in the presence of LY294002 depends on both metabolic and oxygenic status of the cells

LY294002 acts upon PI3K and consequently affects the phosphorylation status of the downstream target, Akt. Akt is activated by phosphorylation within the carboxy terminus at Ser473 and by phospholipid binding and activation loop phosphorylation at Thr308 by PDK1.[12] We therefore investigated the phosphorylation status of Akt from cell lysates collected from both RD and U87 cell lines under either hypoxic or normoxic conditions, and in the presence of increasing concentrations of LY294002. RD cells showed a decrease in phosphorylation of Akt at Ser473 under normoxic (21% oxygen) conditions (Figure 4a; i). Phosphorylation of Akt could be seen to decrease to approximately 15.4% of zero drug control (Figure 4b). However, under hypoxic conditions (1% oxygen) the protein can be seen to be phosphorylated even in the presence of 50 μM drug (Figure 4a; i), equivalent to 59.8% of control (Figure 4b).Therefore, the pathway is not being inhibited by LY294002, consistent with higher cell viability as seen in RD cells under hypoxic conditions (Figure 4b). Conversely, U87 cells showed a decrease in the phosphorylation of Ser 473 under both normoxic and hypoxic conditions (Figure 4a; ii). Under hypoxic conditions at 50 μM, phosphorylation falls to 38.1% of control, whereas under normoxic conditions phosphorylation is even further reduced to 13.6% of control.

Thus, the higher level of AKT phosphorylation following LY294002 treatment in RD cells under hypoxic conditions is aligned with the higher cell viability of this cell line. This suggests that LY294002 may be less effective under hypoxic conditions in cells with a predominantly oxidative phosphorylation (OXPHOS) mechanism.

4. Discussion

It is highly likely that the metabolic profile of cancer cells and substrate availability (e.g. glucose and oxygen) will have a major effect on the growth of cancers *in vivo* and the efficacy of drugs used to treat them. Recent *in vivo* studies have identified glycolytic and OXPHOS sub groups of cancer cells in a variety of cancers including Brain[13], Lymphoma[14] and Liver[15]. We have previously established the base-line bioenergetics phenotype of a number of human cancer cell lines[9] and used this data to choose a more aerobic (RD) and glycolytic (U87) cell line to study with LY294002 (see also supplementary information for ¹³C NMR data). This was in agreement with other reports, where U87 cells were shown to exhibit a glycolytic-dependent phenotype with functional OXPHOS.[16] We therefore investigate the effects of reduced oxygen availability on drug treatment in these two metabolically diverse cell lines.

Low oxygen tension in tumors has also been associated with increased metastasis and poor survival in patients.[17,18] Such conditions may also affect the ways in which chemotherapy drugs act on the cells. We therefore wanted to assess the proliferation rate of cells in the presence of the drug, under both normoxic and hypoxic conditions (1% O_2). To ensure that the drug itself was not altered under the experimental system, the compound was first monitored by ¹H NMR spectroscopy under a variety of conditions: The drug was dissolved in methanol and monitored after 1 hour, 24 hours, 3 days, 7 days and 28 days; the solution was exposed to UV light for 24 hours, and the drug was dissolved in ethanol: PBS (1:3.5) for 24 hours with or without UV exposure, and under 1% oxygen in both solvent systems. We were able to confirm that none of the conditions resulted in a change to the molecule as monitored by NMR spectroscopy (data not shown). Experiments were performed with LY294002 at micro molar concentrations up to 50 μM. This is in line with other studies; for example Lee *et al.*,[19] treated three different hepatocellular carcinoma lines and showed suppressed cell growth with 40 μM LY294002, and Buotempo *et al.*,[20] showed radio-sensitization of two cervical cancer lines with 25 μM LY294002. Data showed that under normoxic conditions, cell death as determined by proliferation was dose-dependent in both cell lines, although U87 cells were more susceptible to the drug. As well as determining proliferation, the viability of cells treated with LY294002 was also assessed using MTT since reduction of the dye only occurs in metabolically active cells and marked changes in metabolic activity can potentially result in significant changes in results despite the fact that the number of viable cells remains constant.[21] Our study, however, confirmed that the same trend was seen in terms of both proliferation and metabolic activity, in both RD and U87 cells. From our data it can be seen that not only do the two cell lines tested show different sensitivity to the drug, but the sensitivity is altered under reduced oxygen conditions. The fact that both cell lines were less susceptible to the drug under hypoxic conditions underlines the importance of using test conditions that are as close as possible to the *in vivo* conditions. This is important *in vivo* since cancerous tissue is often hypoxic due to limited angiogenesis which can compromise normal biological functions.[22]

It has been proposed that increased rates of glucose metabolism in tumor cells are associated with Akt hyperactivation.[23,24] LY294002 acts upon PI3K and consequently affects the phosphorylation status of Akt as a downstream target. These observations have led to the proposal that inhibition of Akt signaling would inhibit glycolysis and increase hydrogen peroxide production which would preferentially kill tumor cells versus normal cells *via* oxidative stress.[25]

Phosphorylation of Akt at Ser 473 in RD cells showed less of a decrease in phosphorylation under both normoxic and hypoxic conditions, than U87. Thus, the higher level of AKT phosphorylation following LY294002 treatment in RD cells under hypoxic conditions is aligned with the higher cell viability of this cell line. This again suggests that LY294002 may be less effective under hypoxic conditions in cells with a predominantly OXPHOS mechanism. Our results are consistent with the hypothesis that a slowing of glycolysis would be expected if the PI3K pathway is inhibited by LY294002. Furthermore, PI3K is a downstream signal mediator of the insulin receptor that activates translocation of the glucose transporter GLUT4, to the cell surface and LY294002 has been reported to reduce levels of the glycolytic enzymes pyruvate kinase M1/M2, fructose-biphosphate aldose A, phosphoglycerate kinase 1, triose phosphate isomerase, and alpha enolase.[26]

To further interrogate the effects on metabolism in the presence of LY294002, the generation of lactate by cells *in vitro* was assessed. Our data indicates that the addition of drug showed significant reductions in lactate generation for the two cell lines under both hypoxic and normoxic conditions. This is in agreement with a previous study in LN18 glioblastoma cells which showed that the presence of the inhibitor LY294002 abolished Akt phosphorylation, and concomitantly inhibited glucose uptake and lactate production.[27]

Although sourced from two different tumor types (U87, adult glioblastoma; RD, paediatric rhabdomyosarcoma) an oncogene screen (Supplementary Figure 2, and Supplementary Table 1) could potentially highlight differences which could be explored in future studies investigating larger cancer panels. Mutations were identified in PTEN 209 G → T in the U87 line and TP53 742 C → T in the RD line (Supplementary Table 2 and 3). Common mutations in the tumor suppressor genes TP53 and PTEN are strongly linked to cellular responses to metabolic energy stress, and the regulation of both glycolysis and oxidative phosphorylation.[28,29] Mutations in both TP53 and PTEN could also affect drug susceptibility with the PTEN mutation in the U87 cell line likely having an impact on susceptibility to PI3K inhibitors.[30] Other mutations that were identified include an NRAS 183 A → T (RD) and a CDKN2A deletion (U87) (Supplementary Table 2). The NRAS mutation in the RD line could be linked to its reduced sensitivity to LY294002 and its high level of mitochondrial respiration. KRAS mutations have been shown able to unregulated glucose uptake when glycolysis is inhibited[31] and maintain high levels of mitochondrial oxidative metabolism.[32,33] Mutations in cyclin dependent kinases such as CDKN2A although linked to uncontrolled proliferation are unlikely to be linked to differences in metabolism and responses to PI3K inhibitors.

5. Conclusion

In conclusion, the drug can be seen to have affected the two cell lines tested to dramatically different extents. Metabolic profiling to determine which cells *in vivo* will be treatable by a drug is likely to become increasingly important. Tumors *in vivo* appear to be heterogeneous in terms of their energy metabolism, with cancer cells using both glycolysis and oxidative phosphorylation. In time it is possible that bioenergetics profiling of tumors from biopsy materials will enable drugs, and combinations of drugs, to be specifically selected for a particular cancer type or group of patients.

Conflict of Interest

The authors declare that they have no conflicts of interest. The authors alone are responsible for the content and writing of the paper.

References

1. Abbott B, Thompson P. Synthetic studies of the phosphatidylinositol 3-Kinase inhibitor LY294002 and related analogues. Aust. J. Chem. 2003;56:1099-106.
2. Hanahan D, Weinberg RA. Hallmarks of cancer: the next generation. Cell. 2011;144:646-74.
3. Gogvadze V, Orrenius S, Zhivotovsky B. Mitochondria in cancer cells: what is so special about them? Trends Cell Biol. 2008;18(4):165-73.
4. Obre E, Rossignol R. Emerging concepts in bioenergetics and cancer research: metabolic flexibility, coupling, symbiosis, switch, oxidative tumors, metabolic remodeling, signaling and bioenergetics therapy. Int J Biochem Cell Biol. 2015;59:167-81.
5. Vlahos CJ, Matter WF, Hui KY, *et al*. A Specific Inhibitor of Phosphatidylinositol 3-Kinase 2-(4-Morpholinyl)-8-phenyl-4H-l-benzopyran-4-one (LY294002). J Biol Chem.1994; 269: 5241-8.
6. Andjelkovic M, Alessi DR, Meier R, *et al*. Role of translocation in the activation and function of protein kinase B. J Biol Chem. 1997;272:31515-24.
7. Bellacosa A, Chan TO, Ahmed NN, *et al*. Akt activation by growth factors is a multiple step process; the role of the PH domain. Oncogen. 1998;17:313-25.
8. Sarbassov DD, Guertin DA, Ali SM, *et al*. Phosphorylation and regulation of Akt/PKB by the rictor-mTOR complex. Science. 2005;307:1098-101.
9. Potter M, Newport E, and Morten KJ. The Warburg Effect: 80 Years on. Biochem Soc Trans. 2016;44(5):1499-505.

10. Brown JM, Wilson WR. Exploiting tumor hypoxia in cancer treatment. Nat Rev Cancer. 2004;4:437-47.
11. Zhao Y, Butler EB, Tan M. Targeting cellular metabolism to improve cancer therapeutics. Cell Death Dis. 2013; 4:e532.
12. Alessi DR, Andjelkovic M, Caudwell B, *et al*. Mechanism of activation of protein kinase B by insulin and IGF-1. EMBO J. 1996;15:6541-51.
13. Marin-Valencia I, Yang C, Mashimo T, *et al*. Analysis of tumor metabolism reveals mitochondrial glucose oxidation in genetically diverse human glioblastomas in the mouse brain in vivo. Cell Metab. 2012;15:827-37.
14. Caro P, Kishan AU, Norberg E, *et al*. Metabolic signatures uncover distinct targets in molecular subsets of diffuse large B-Cell Lymphoma. Cancer Cell. 2012;22:547–60.
15. Morton R, Cunningham C, Jester R, *et al*. Alteration of mitochondrial function and lipid composition in Morris 7777 Hepatoma. Cancer Res. 1976;36:3246.
16. Griguer CE, Oliva CR, Gillespie GY. Glucose metabolism heterogeneity in human and mouse malignant glioma cell lines. J Neuro-Oncology. 2005;74:123–33.
17. Hockel M, Schlenger K, Hockel S, *et al*. Hypoxic cervical cancers with low apoptotic index are highly aggressive. Cancer Res. 1999;59:4525–8.
18. Hockel M, Vaupel P. Tumor hypoxia: definitions and current clinical, biologic, and molecular aspects. J. Natl Cancer Inst. 2001;93:266–76.
19. Lee CM, Fuhrman CB, Planelles V, *et al*. Phosphatidylinositol 3-Kinase inhibition by LY294002 radio sensitizes human cervical cancer cell lines. Clin Cancer Res. 2006;12:250-6.
20. Buontempo F, Ersahin T, Missiroli S, *et al*. Inhibition of akt signaling in hepatoma cells induces apoptotic cell death independent of akt activation status. Invest New Drugs. 2011;29:1303-13.
21. Vega-Avila E, Pugsley MK. An overview of colorimetric assay methods used to assess survival or proliferation of mammalian cells. Proc. West. Pharmacol. Soc. 2011;54:10-4.
22. Olin MR, Anderson BM, Litterman AJ, *et al.* Oxygen is a master regulator of the immunogenicity of primary human glioma cells. Cancer Res. 2011;71:6583-9.
23. Amornphimoltham P, Sriuranpong V, Patel V, *et al*. Persistent activation of the Akt pathway in head and neck squamous cell carcinoma: a potential target for UCN-01. Clin Cancer Res. 2004;10:4029-37.
24. Pedrero JM, Carracedo DG, Pinto CM, *et al*. Frequent genetic and biochemical alterations of the PI 3-K/AKT/PTEN pathway in head and neck squamous cell carcinoma. Int J Cancer. 2005;114:242-8.
25. Simons AL, Orcutt KP, Madsen JM, *et al*. The Role of Akt pathway signaling in glucose metabolism and metabolic oxidative stress in oxidative stress in cancer biology and therapy, D.R. Spitz *et al*. (eds.). Springer. 2012.
26. Mallawaaratchy DM, Mactier S, Kaufman KL, *et al*. The phosphoinositide 3-kinase inhibitor LY294002, decreases aminoacyl-tRNA synthetases, chaperones and glycolytic enzymes in human HT-29 colorectal cancer cells. J Proteomics. 2011;75:1590-9.
27. Elstrom R, Bauer DE, Buzzai M, *et al*. Akt stimulates aerobic glycolysis in cancer cells. Cancer Res. 2004; 64:3892-9.
28. Vousden KH, Ryan KM. p53 and metabolism. Nat Rev Cancer. 2009;9(10):691-700.
29. Garcia-Cao I, Song MS, Hobbs RM, *et al*. Systemic elevation of PTEN induces a tumor-suppressive metabolic state. Cell. 2012;49:49-62.
30. Papa A, Wan L, Bonora M, *et al*. Cancer-associated PTEN mutants act in a dominant-negative manner to suppress PTEN protein function. Cell. 2014;157:595-610.
31. Yun J, Rago C, Cheong I, *et al*. Glucose deprivation contributes to the development of KRAS pathway mutations in tumor cells. Science. 2009;325:1555-9.
32. Guo JY, Chen H-Y, Mathew R, *et al*. Activated Ras requires autophagy to maintain oxidative metabolism and tumorigenesis. Genes Dev. 2011;25;460-70.
33. Weinberg F, Hamanaka R, Wheaton WW, *et al*. Mitochondrial metabolism and ROS generation are essential for Kras-mediated tumorigenicity. Proc Natl Acad Sci. 2010;107(19):8788-93.

SUPPLEMENTARY INFORMATION

1. Methods and Materials
1.1. Nuclear magnetic resonance spectroscopy (NMR)
Cells were fed with DMEM supplemented with 2 mM L-glutamine, 1 mM pyruvate and 20 mM D-[U-^{13}C] glucose (UK Isotope) for 2 hours. After 2 hours cells were washed with ice cold PBS. Cells were then scraped over dry ice and extracted with a 55:35:10 mix of MeCN: MeOH: double distilled H_2O. Samples were vortexes, centrifuged and the supernatant freeze dried. Lyophilised products were reconstituted in 50mM sodium phosphate buffer (pH 7) containing 500 µM TSP, 1.5 mM sodium azide and 10% D_2O (Sigma).

^{13}C NMR spectra were collected on a Bruker AVIII 700 spectrometer equipped with a He-cooled TCI cryoprobe with sample temperatures stabilized at 298K in 5 mm NMR tubes. Pulse excitation used a 3.6 µs (30°) ^{13}C pulse and power gated proton decoupling was achieved with a WALTZ-16 scheme employing 80 µs ^{1}H 90° pulses during the 0.8 s acquisition period. Data accumulations consisted of between 2000 - 10240 transients per 1D spectrum. All spectra were processed using a 1Hz exponential line broadening (LB = 1 Hz).

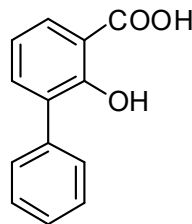### 1.2. Next Generation sequencing
Next Generation Sequencing (NGS) analysis was performed on 50 known oncogene and tumor suppressor genes. Analysis was carried out by NIM Genetics (Madrid) and involved an initial enrichment, by multiplex PCR, of selected regions of oncogenes and tumor suppressor genes which make up the Ion AmpliSeq™ HotSpot Cancer Panel v2 (Figure S1). NGS of the enriched sample, and subsequent data analysis, were performed to identify mutations affecting these regions, with specific attention to 2855 hotspot mutation sites. NGS was carried out using the ION Torrent Personal Genome Machine (Life Technologies). The obtained reads were then aligned to the Human genome (build 37hg19) using the TMAP aligner v.3.63-1 (Life Technologies). Variants were called using Variant Caller v.3.6.59049 (Life Technologies). Briefly, aligned sequences were filtered based on quality and mapping scores before being analyzed for differences between the obtained sequence and the reference sequence. The variant calls were further evaluated using the following databases: dbSNP the 1000 genomes project, and the Exome Variant Server. This showed whether a given variant is present in the general population at polymorphic frequencies (1% or greater) and has not been associated with disease. The COSMIC database was then consulted to annotate any variants that were called in the samples and found in the database. Finally, each variant was analysed using the Variant Effect Predictor and PROVEAN tools to establish the predicted biological effect. Splice site statistical analysis was performed using ALAMUT (Interactive-Biosoftware). The sequencing panel has been designed to specifically target mutational hotspots that are frequently mutated in human cancers. Mutations at other sites in the 207 amplicons may not be detected with the same level of sensitivity. The target genes are not sequenced in their entirety and therefore mutations that are not present in the sequenced regions will not be detected. The limit of somatic mutation detection is 5% at a depth of coverage of 500x.

1.3. Synthesis route for LY294002
Step (i): 3-phenyl salicaldehyde (2)

(2) was synthesized from commercially available 2-phenyl phenol (1) by ortho-formylation (Hoffsloken & Skattebol, 1999). To solution (0.20 M) of (1) 1 eqv. in dried THF was added Et$_3$N (2 eqv.), MgCl$_2$ (2 eqv.) and paraformaldehyde (5 eqv.) respectively. The reaction mixture was stirred for 2 hours, reflux at 70 °C. NMR of crude showed 90% or more conversion. Crude was subjected to step 2 without purification.
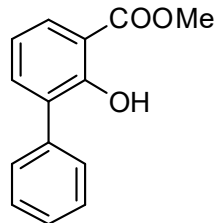
Step (ii): 3-phenyl salicylic acid (3)

(3) was an oxidation product of (2) from Pinnick-like oxidation (Kang *et al*., 2003). To solution of (2) (1 eqv., 1.16 g, 5.86 mmol) in dimethyl sufoxide (17.8 mL) was added NaH$_2$PO$_4$(aq) (2.5 eqv., 1.64 g) and NaClO$_2$(aq) (2.5 eqv. , 1.32 g) at 0 °C. The reaction mixture was slowly warmed up to room temperature and stirred overnight then additional
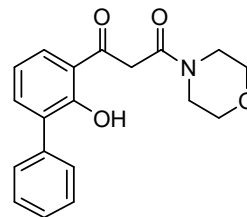
NaH$_2$PO$_4$(aq) (1 eqv., 703 mg) and NaClO$_2$(aq) (1 eqv., 523 mg) were added at 0 °C and stirred overnight. The reaction mixture was acidified by 1 M HCl and was extracted by ethyl acetate. The organic layer was dried over NaSO$_4$(s), filtered and solvent was removed under vacuum. Column chromatography (gradient, 3:1:0.1 = petroleum ether : ethyl acetate : acetic acid) of the concentrated crude resulted off-white solid (476 mg, 41% yield) m.p. 186 - 188 °C Melting point was consistent with those previously reported (Brooks *et al.*, 1961). No NMR spectra have been published.

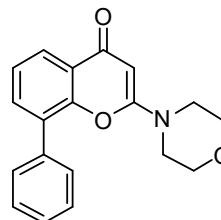Step (iii): methyl 2-hydroxy-[1,1'-biphenyl]-3-carboxylate (4)

Ester **(4)** was synthesized from **(3)** by esterification. To solution of **(3)** (476 mg, 2.22 mmol) in anhydrous methanol (156 mL) was added H$_2$SO$_4$ (15.6 mL). The reaction mixture was stirred and heated to reflux at 85 °C for two days. The reaction mixture was then cooled to room temperature before neutralized by NaH$_2$CO$_3$(aq) (2.9 - 3.5 M) and was extracted by ethyl acetate. The extract was dried over NaSO$_4$(s), filtered and solvent was removed under vacuum to afford colorless oil which crystallizes upon standing (453 mg 1.98 mmol, 89.4% yield).

Step (iv): 1-(2-hydroxy-[1,1'-biphenyl]-3-yl)-3-morpholinopropane-1,3-dione (5)

(5) was synthesized from **(4)** by claisen-like reaction (Griffin *et al.*, 2005). Dried tetrahydrofuran (3 mL) was added 18 M lithium, diisopropylamide (0.42 mL) and 4-acetylmorpholine (43.9 µL). The reaction mixture was stirred at room temperature for 30 minutes before addition of solution of (4) (54.1 mg) in dried tetrahydrofuran (3 mL). The reaction mixture was left to stir at room temperature overnight. The reaction mixture was neutralized by 1 M HCl and was extracted by CH$_2$Cl$_2$. The extract was dried over NaSO$_4$(s), filtered and solvent was removed under vacuum to afford yellow oil. The concentrated crude was purified by column chromatography to give off-white solid **(5)** (49.3 mg, 64% yield) ^{1}H NMR (250 MHz, CDCl$_3$) $\square_\square$: 12.44 (1 H, s), 7.88 (1 H, dd, 7.9, 1.8), 7.54 - 7.60 (3 H, m), 7.33 - 7.48 (3 H, m), 7.02 (1 H, t, *J* 7.8), 4.18 (2 H, s), 3.72-3.68 (6 H, m), 3.56 - 3.51 (2 H, m) ^{13}C NMR (CDCl3) δc: 200, 164.8, 160.1 138.0, 136.6, 131.4, 130.2, 129.3, 128.2, 127.5, 119.2, 119.1, 66.7, 66.5, 47.0, 45.5, 42.4. ^{1}H NMR data was consistent with those previously reported[4] no data about ^{13}C NMR previously reported.

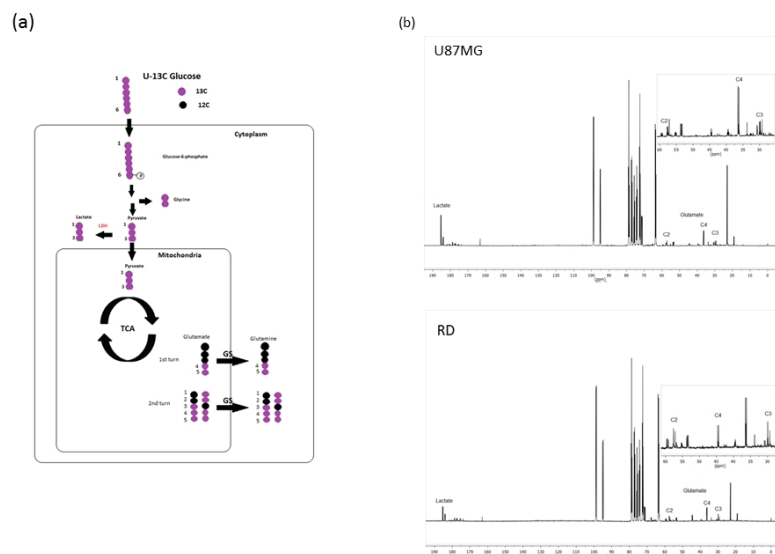Step (v): 2-morpholino-8-phenyl-4H-chromen-4-one (6)

(6) was obtained from **(5)** by cyclodehydration (Zhou *et al.*, 2008). To solution of **(5)** (49.3 mg, 0.15 mmol) in dried CH$_2$Cl$_2$ (0.75 mL) was added triflic anhydride (91.8 µL). The reaction mixture was stirred overnight then concentrated under vacuum. Anhydrous methanol (10 mL) was added to reaction mixture and was stirred for 4 hours. The reaction mixture was neutralized by NaHCO$_3$(aq) and extracted by CH$_2$Cl$_2$. The organic layer was dried over Na$_2$SO$_4$(s), filtered and solvent was removed under vacuum. The crude reaction mixture was purified by column chromatography to give off-white solid **(6)** (25.3 mg, 55% yield)) ^{1}H NMR (500 MHz, CDCl$_3$) δH: 8.17 (1 H, dd, *J* 7.9, 1.6), 7.56 (1 H, dd, *J* 7.3, 1.6), 7.51-7.38 (6 H, m), 5.50 (1 H, s), 3.71 (2 H, t, *J* 4.9), 3.3 (3 H, t, *J* 4.8) ^{13}C NMR (500 MHz,CDCl3) δC: 177.2, 162.5, 150.5, 136.3, 133.4, 130.3, 129.3, 128.3, 128.0, 125.0, 124.7, 123.3, 87.0, 65.9, 44.7.

2. Results

2.1. 13C-NMR studies

The metabolic status of the two chosen cell lines was characterized by ^{13}C-NMR. Figure S1 illustrates the potential fate of universally labeled glucose, depicting how it is metabolized through the glycolytic pathway to lactate or through pyruvate into the TCA cycle. Glycolysis will produce pyruvate and lactate molecules that are labeled in all three-carbon positions. If the TCA cycle is functioning normally (active PDH), then after the first cycle glutamine and glutamate doublets labeled in the 4-5 position can be seen. This labeling can only occur if PDH and the TCA cycle result in glucose oxidation via the mitochondria. As the TCA cycle completes further cycles other multiplet labeling patterns are seen (in 3, 4 and 5 carbon positions) and evidence of complete turnover of the cycle is confirmed by double doublets (quartets) in glutamine and glutamate C4 position.[17]

The addition of U-^{13}C glucose to U87 (glycolytic) and RD (aerobic) cell extracts revealed many similarities between the two cell lines with spectra showing multiple peaks of ^{13}C labeled metabolites. Close examination of the spectra showed that there was significant TCA cycle activity in both cell lines. The NMR spectra show glutamate 4-5 doublets in both U87 and RD cell lines. The U87 extract also shows double doublets (Q435) which are generated from complete turnover of the TCA cycle. To the contrary, the RD extract contained the doublets but not the quartets; the reason for this is still unknown. Glutamine labeling was also observed and was similar for both lines (data not shown). Large lactate peaks were seen for the U87 but also for the RD cell line, which had shown a more aerobic energy profile (Supplementary Figures 1 b&c). As internal standards were not used in these experiments the concentrations of lactate cannot be quantified with peak sizes only giving relative amounts. The lactate peaks in the RD extracts were a little unexpected given their aerobic nature and low levels of lactate production (Figure 3).

Supplementary Figure S1: (a) Schematic depicting the possible fate of U13 C labeled glucose in the cell; adapted from Marin Valencia *et al.*, 2012 (b) Whole 1D-NMR spectrum of U^{13}C labeled glucose metabolites in U87 and RD cells; inlay shows glutamate metabolites in more detail (c) Higher resolution spectra of Glutamate C2, C3 and C4 metabolites.

The U87 glioblastoma cell line showed a significant amount of glucose oxidation. However, this oxidation is not linked to respiratory chain ATP production. It is possible that U87 cells generate high levels of lactate due to an increase in glycolysis linked to the inability to couple TCA cycle activity to mitochondrial respiration. The metabolomics data coupled with the data from the metabolic assays suggests that both glycolysis and glucose oxidation are equally important for U87 cells; glycolysis perhaps providing ATP, and glucose oxidation providing intermediates for macromolecule synthesis. While the mitochondria in U87 cells are not being utilized for energy it is clear that they are active in their TCA cycling, presumably as a means of meeting the biosynthetic demands required to provide accelerated growth.[28] The glycolytic rate in RD cells appears lower than U87 but energy production via mitochondrial respiration appears more efficient. RD cells with higher levels of mitochondrial respiration could potentially use other

substrates (i.e. fatty acids and glutamate) to generate ATP if glycolysis is impaired. Under hypoxic conditions with high concentration of glucose (20 mM), the RD cell line will likely be more impaired than the U87 cell line as it appears reliant on mitochondrial respiration. The U87 line with its high level of glycolysis might show very little effects of hypoxic growth. A compound which inhibits glycolysis is likely to have a significant effect on the U87 cells under normoxic conditions as these cells appear reliant on high rates of glycolysis to generate ATP.

2.2. Gene sequencing

The sequencing libraries generated from the U87 and RD cell lines were sequenced to an average depth of 3023 and 3398 respectively, resulting in 97.42% and 97.05% of bases included in the panel being sequenced to a depth of at least 500x. In the U87 cell line one hot spot mutation was identified in the PTEN gene (Supplementary Table 2).
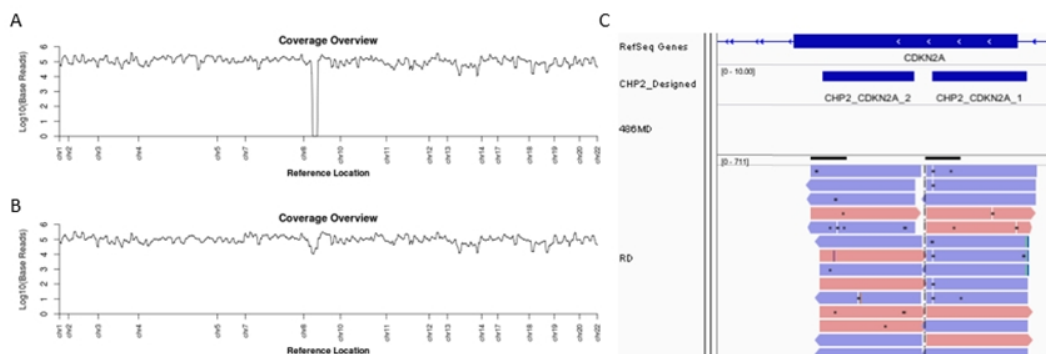
ABL1	BRAF	FBXW7	FGFR1	GNAQ	IDH2	KRAS	NPM1	PTPN11	SMO
AKT1	CDH1	EGFR	FGFR2	GNAS	JAK2	MET	NRAS	RB1	SRC
ALK	CDKN2A	ERBB2	FGFR3	HNF1A	JAK3	MLH1	PDGFRA	RET	STK11
APC	CSF1R	ERBB4	FLT3	HRAS	KDR	MPL	PIK3CA	SMAD4	TP53
ATM	CTNNB1	EZH2	GNA11	IDH1	KIT	NOTCH1	PTEN	SMARCB1	VHL

Supplementary Table S1: List of the 50 oncogenes and tumor suppressor genes included in the Ion AmpliSeq TM HotSpot cancer panel v2

Cell Line	Chr.	Position	Gene	Ref. Allele	Variant Allele	Var. Freq.	Cov.	COSMIC	Transcript	Nucleotide Change	Amino Acid Change	Effect
U87-MG	10	89685315	PTEN	G	T	100	1166	-	NM_000314.4	c.209+1G>T	-	3' Splice Site
RD	1	115256528	NRAS	A	T	62.3	1994	COSM585	NM_002524.3	c.183A>T	Missense	p.Gln61His
RD	17	7577539	TP53	C	T	100	1992	COSM10656	NM_000546.4	c.742C>T	Missense	p.Arg248Trp

Supplementary Table S2: Non-polymorphic changes identified in cell lines U87 and RD. The reference allele (Ref. Allele) and variant allele are both listed in the table. "Var. Freq." refers to the variant frequency in the sequenced reads, which is representative of the population of cells sequenced. "Cov" refers to the sequence coverage i.e. the number of times the position has been sequenced. A splice site variant was identified in the U87 cell line and two missense mutations in the RD line. The RD line mutations are present in the COSMIC database and their COSMIC IDs are included in the table.

This mutation at C209 G > T is located in the intron 3 splice site of the PTEN gene. An *in-silico* prediction of splicing was performed using the available algorithms (SSF, MaxEnt, NNSPLICE, GeneSplicer and HSF) in ALAMUT (Interactive-Biosoftware, Rouen, France).

Supplementary Figure S2: Coverage overview plots of sample (a) U87, and (b) RD. An absence of coverage in chromosome 9 indicates a homozygous deletion in U87 but due to the design of the sequencing experiment it is not

possible to identify the coordinates of the breakpoints. The IGV image (c) shows sequencing reads from the same two samples in the affected exon 3 of CDKN2A. No sequencing reads are observed in sample U87.

A significant change in the donor site is predicted (Supplementary Table 3). In addition coverage analysis performed on the sequencing results showed a lack of coverage of chromosome 9 for the U87 sample (Supplementary Figure 2a).

Location	Mutation	SSF [0-100] ≥ 70	MaxEnt [0-12] ≥ 0	NNSPLICE [0-1] ≥ 0.4	HSF [0-100] ≥ 65
Exon 3 c.209	c.209+1G>T	73.34	7.96	0.95	82.40

Supplementary Table S3: Results of splice site analysis, performed in Alamut. Four algorithms were used to evaluate the effect of the c209 + 1 G → T mutation. Analysis with SSF, MaxEnt, NNSPLICE and HSF all predicted a deleterious effect on splicing. Ranges of possible values are in square brackets and the significance thresholds can be found in italics. Values greater than the threshold predict a deleterious effect.

This was confirmed visually in IGV and affects the CDKN2A gene (Supplementary Figure 2c). This is most likely caused by a homozygous deletion in the region however due to the design of the sequencing experiment it is not possible to identify the coordinates of the break point.